SCIENTIFIC REPORTS
nature research

Corrected: Author Correction

OPEN

Structure, optical and magnetic properties of new $Bi_{0.5}Na_{0.5}TiO_3$-$SrMnO_{3-\delta}$ solid solution materials

Dang Duc Dung[1*], Nguyen The Hung[1,2] & Dorj Odkhuu[3*]

The new $Bi_{0.5}Na_{0.5}TiO_3$-$SrMnO_{3-\delta}$ solid solution materials were fabricated via sol–gel method. The random incorporation of Sr and Mn cations into host lattice of $Bi_{0.5}Na_{0.5}TiO_3$ resulted in structural distortion and influenced on the reduction of the optical band gap from 3.07 eV to 1.81 eV for pure $Bi_{0.5}Na_{0.5}TiO_3$ and 9 mol% $SrMnO_{3-\delta}$ solid solution into $Bi_{0.5}Na_{0.5}TiO_3$. The magnetic properties of $Bi_{0.5}Na_{0.5}TiO_3$ materials at room temperature were tuned via compensation of diamagnetic material with weak-ferromagnetism to ferromagnetism with low $SrMnO_{3-\delta}$ content and combination of paramagnetism/antiferromagnetism-like and ferromagnetism with higher $SrMnO_{3-\delta}$ content solid solution in $Bi_{0.5}Na_{0.5}TiO_3$. The tunable magnetic and optical properties of lead-free ferroelectric materials was promising for their application to green electronic devices.

$Bi_{0.5}Na_{0.5}TiO_3$ materials and their solid solution showed rapid development, especially in the search of high-performance lead-free piezoelectric materials to address human health and environmental protection concerns[1,2]. $Bi_{0.5}Na_{0.5}TiO_3$ material which was firstly fabricated by Smolenskii *et al.* in 1961, is an *A*-site complex perovskite-structured material with random distribution of Bi and Na cation at *A*-site[3]. At room temperature, $Bi_{0.5}Na_{0.5}TiO_3$ materials has a rhombohedral symmetry with Curie temperature (T_C) ~320 °C, remanence polarization (P_r) ~38 μC/cm^2, high dielectric constant (ε_r ~694 at 1 kHz) and low dielectric loss (tanδ ~0.103) while high coercive field ~7.3 kV/mm, thereby resulting in weak piezoelectric coefficient (d_{33}) ~73–80 pC/N due to hard to polling treatment[4,5]. The $Bi_{0.5}Na_{0.5}TiO_3$ materials displayed a direct transition optical band gap (E_g~3.01–3.18 eV), depending on the fabrication method[6]. However, the performance properties of lead-free ferroelectric $Bi_{0.5}Na_{0.5}TiO_3$ materials are still not comparable with those of Pb(Ti,Zr)O_3-based materials in terms of application requirements in electronic devices[7,8]. The high-performance properties of lead-free ferroelectric $Bi_{0.5}Na_{0.5}TiO_3$ materials were recently greatly enhanced by using a solid solution with various compounds containing transition metal such as $BiCoO_3$, $Bi(Zn_{0.5}Hf_{0.5})O_3$, $Bi(Mn_{0.5}Ti_{0.5})O_3$, $Bi(Co_{0.5}Ti_{0.5})O_3$ etc.[4,9–12]. Guo *et al.* reported that $BiCoO_3$-modified $Bi_{0.5}Na_{0.5}TiO_3$ materials were exhibited the increasing d_{33} values up to 107 pC/N, whereas and the coercive field were reduced to 5.25 kV/mm[4]. The $Bi(Zn_{0.5}Hf_{0.5})O_3$-modified $Bi_{0.5}Na_{0.5}TiO_3$ materials increased the P_r and T_C values to 43.5 μC/cm^2 and 340 °C, respectively[9]. $Bi(Mn_{0.5}Ti_{0.5})O_3$ and $Bi(Co_{0.5}Ti_{0.5})O_3$ solid solution into $Bi_{0.5}Na_{0.5}TiO_3$-based materials resulted in a display a giant electrical field-induced strain coefficient values (d^*_{33}) to 818 pm/V and 600 pm/V, respectively[10–12]. In addition, the *A*-site was modified $Bi_{0.5}Na_{0.5}TiO_3$ materials via Sr as solid solution of $SrTiO_3$ in $Bi_{0.5}Na_{0.5}TiO_3$ materials, a large electrical field-induced strain of over 1000 pm/V for low-driving fields (less than 2 kV/mm) was achieved[13]. The solid solution with perovskite-type material containing the transition metal and alkaline cations possibly enhanced the performance of electrical properties of lead-free ferroelectric $Bi_{0.5}Na_{0.5}TiO_3$-based materials.

The observation of room temperature ferromagnetism in pure $Bi_{0.5}Na_{0.5}TiO_3$ materials was promising for the transfer of lead-free ferroelectric material to multiferroic applications in electronic devices[14–17]. Ju *et al.* obtained the room temperature ferromagnetism in nanocrystalline $Bi_{0.5}Na_{0.5}TiO_3$ and its possible origin from Na vacancies located at/near surface of nanograins[14]. Thanh *et al.* also achieved the room temperature ferromagnetism versus diamagnetism in pure $Bi_{0.5}Na_{0.5}TiO_3$ materials[15,16]. Zhang *et al.* predicted the ideal $Bi_{0.5}Na_{0.5}TiO_3$ non-magnetic material; whereas Na or Ti vacancies can induce the magnetism rather than Bi or O vacancies by using ab initio calculations[17]. However, the main problem of magnetism in pure $Bi_{0.5}Na_{0.5}TiO_3$ compounds is low magnetisation (less than 1 memu/g) and strong influence of diamagnetic components, which were raised from empty orbital of

[1]Department of General Physics, School of Engineering Physics, Ha Noi University of Science and Technology, 1 Dai Co Viet road, Ha Noi, Viet Nam. [2]Department of Physics, Faculty of Basic and Fundamental Sciences, Viet Nam Maritime University, 484, Lach Tray street, Hai Phong city, Viet Nam. [3]Department of Physics, Incheon National University, Incheon, 22012, Republic of Korea. *email: dung.dangduc@hust.edu.vn; odkhuu@inu.ac.kr

$3d^0$-Ti[14–16]. Therefore, for a new $Bi_{0.5}Na_{0.5}TiO_3$-based compound is important for the transfer of the materials to industrial application in smart electronic devices. Simple ideas were used for investigating high ferromagnetism at room temperature; transition metal was used as impurities for substitution at Ti-site in perovskite structure. Room temperature ferromagnetism in $Bi_{0.5}Na_{0.5}TiO_3$ was reported for Co-, Mn-, Ni-, Fe- and Cr-dopants[15,16,18–20]. However, the physical property of room temperature ferromagnetism ordering phenomenal was raised from various parameters, was not well understood. The room temperature ferromagnetism in Mn-, Ni- and Fe-doped $Bi_{0.5}Na_{0.5}TiO_3$ compounds are intrinsic phenomena that resulting from the interaction between magnetic ions through the oxygen vacancies[16,18,20]. It is unlikely that the room temperature ferromagnetism in Cr-doped $Bi_{0.5}Na_{0.5}TiO_3$ compound originated more from oxygen vacancies than the interaction of Cr ions, whereas ferromagnetism in Co-doped $Bi_{0.5}Na_{0.5}TiO_3$ compound was exhibited from magnetic Co clusters[15,19]. The other method was used in tailoring ferromagnetic properties in lead-free ferroelectric $Bi_{0.5}Na_{0.5}TiO_3$ materials that sintered the ferroelectric-ferromagnetic materials as composites, such as $CoFe_2O_4/Bi_{0.5}Na_{0.5}TiO_3$ and $MgFe_2O_4/Bi_{0.5}Na_{0.5}TiO_3$[21,22]. However, the main problem of the other method is the pole under low-electrical field during high conductivity of spinel and/or interface effect, which results in large leakage current[23]. Recently, we proposed the new method for arching the room temperature of solid solution with alkaline-transition compounds such as $MgFeO_{3-\delta}$ or $SrFeO_{3-\delta}$[24,25]. In the solid solution, both *A*- and *B*-sites of $Bi_{0.5}Na_{0.5}TiO_3$ compounds were modified by alkaline cation and transition metal ions, respectively, thereby resulting display ferromagnetism with large magnetisation at room temperature and overcoming the single transition metal dopants.

To date, no reports on the use of Mn-based alkaline material as solid solution in $Bi_{0.5}Na_{0.5}TiO_3$ materials are available. Alkaline-earth metal manganese double oxides are interesting materials because oxygen deficiency can be modulated according to their structural, electrical, and magnetic properties[26–30]. Kobayashi *et al.* reported that $SrMnO_3$ and $SrMnO_{2.5}$ compound exhibited the cubic and orthorhombic structure[27]. Hexagonal $SrMnO_3$ was possibly transformed into the pseudocubic $SrMnO_{3-\delta}$ by introducing oxygen vacancies and final reducing state to orthorhombic $SrMnO_{2.5}$ structural[27]. The valence state of Mn near the interface gradually varied from Mn^{3+} to Mn^{4+} over an area of a few atomic layers[27]. Belik *et al.* reported that the polymorphous crystal structures of hexagonal 6H-$SrMnO_3$, hexagonal 4H-$SrMnO_3$, and cubic $SrMnO_3$ have the same chemical composition as $SrMnO_3$[28]. Suescun *et al.* reported that oxygen vacancies ordering in oxygen-deficient perovskites $SrMnO_{3-\delta}$ compounds were possibly reduced to $SrMnO_{2.6}$ and $SrMnO_{2.74}$ with tetragonal and monoclinic properties, respectively[28]. The 6H-$SrMnO_3$, 4H-$SrMnO_3$, and cubic-$SrMnO_3$ exhibited the antiferromagnetic property with Neel temperatures (T_N) of 235 K, 280 K, and 240 K, respectively[27]. The cubic-$SrMnO_3$ exhibited a *G*-type antiferromagnetic structure with T_N in the range 230–260 K probably because of the small variations in oxygen stoichiometry[28,30]. Rahman *et al.* predicted that $SrMnO_2$ is a tetragonal lattice structure with an *A*-type antiferromagnetic conductor[31]. Given the well solid solution of $SrMnO_{3-\delta}$ into host $Bi_{0.5}Na_{0.5}TiO_3$ crystal, we expected that the Sr and Mn cations were diffused to randomly incorporate with the host lattice of $Bi_{0.5}Na_{0.5}TiO_3$ crystal to form a solid solution. Thus, the interaction between random magnetic Mn cations at the *B*-site and co-modified by Sr cations at the *A*-site in host $Bi_{0.5}Na_{0.5}TiO_3$ materials was expected to be of phenomenal interest. In this work, the solid solution of $(1-x)$ $Bi_{0.5}Na_{0.5}TiO_3 + xSrMnO_{3-\delta}$ compounds was fabricated using sol–gel method. The solid solution $SrMnO_{3-\delta}$ in $Bi_{0.5}Na_{0.5}TiO_3$ compound reduced the optical band gap and tunable magnetic properties of host materials.

Results

Chemical compositions. The chemical composition of pure $Bi_{0.5}Na_{0.5}TiO_3$ and $SrMnO_{3-\delta}$-modified $Bi_{0.5}Na_{0.5}TiO_3$ materials were confirmed, as shown in Fig. 1(a,b) for the energy dispersive X-ray spectra of pure and 5 mol% $SrMnO_{3-\delta}$-modified $Bi_{0.5}Na_{0.5}TiO_3$ compounds, respectively, wherein which the selected area for the characterisation element was shown in the inset of each figure. The results showed that the all expectations of elements such as Bi, Na, Ti and O were obtained in pure $Bi_{0.5}Na_{0.5}TiO_3$ as shown in Fig. 1(a). The EDX spectra of $SrMnO_{3-\delta}$-modified $Bi_{0.5}Na_{0.5}TiO_3$ compounds showed the spectral addition elements such as Sr and Mn tailoring with elements Bi, Ti, Na and O host $Bi_{0.5}Na_{0.5}TiO_3$ compounds.

Surface morphologies. The solid solution of $SrMnO_{3-\delta}$ into host $Bi_{0.5}Na_{0.5}TiO_3$ materials resulted in modification of the surface morphologies of samples where the surface morphologies were exhibited inhomogeneous as increasing the $SrMnO_{3-\delta}$ amounts solution. Figure 2(a–g) show the surface morphology of pure $Bi_{0.5}Na_{0.5}TiO_3$ samples and $SrMnO_{3-\delta}$-modified $Bi_{0.5}Na_{0.5}TiO_3$ samples with 0.5, 1, 3, 5, 7, and 9 mol%, respectively. The surface morphology of pure $Bi_{0.5}Na_{0.5}TiO_3$ materials exhibited cubic-like shape with grain size of approximately 3–4 μm, as shown in Fig. 2(a). The minimal addition of 0.5 and 1 mol% $SrMnO_{3-\delta}$ into host $Bi_{0.5}Na_{0.5}TiO_3$ materials resulted in inhomogeneous structure with grain size ranging from 1 μm to 4 μm, as shown in Fig. 2(b,c), respectively. Further addition of $SrMnO_{3-\delta}$ into host $Bi_{0.5}Na_{0.5}TiO_3$ materials with $SrMnO_{3-\delta}$ up to 9 mol% as solid solution reduced the grain size and inhomogeneous distribution of the grain in a wide range from several hundred nanometers to few micrometers, as shown in Fig. 2(d–g). Normally, the presentation of impurities near the grain boundaries resulted in decreasing their mobility substantially as densification occurs. Therefore, small grain size is formed because of the reduction in the mobility of the grain boundary weakens the mass transport, resulting in obviously inhibited grain growth[32,33]. However, the grain size possibly increased because the presentation of oxygen vacancies is beneficial to mass transport during sintering[32,33]. Therefore, we suggested that the combination of both impurities and oxygen vacancy parameter affected the grain growth of $SrMnO_{3-\delta}$-modified $Bi_{0.5}Na_{0.5}TiO_3$ samples, wherein Sr and Mn impurities cations showed inhibited grain growth, whereas oxygen vacancies promoted grain growth.

Room temperature structure. The structural studied in $SrMnO_{3-\delta}$-modified $Bi_{0.5}Na_{0.5}TiO_3$ compound with $SrMnO_{3-\delta}$ concentration up to 9 mol.% were provided that the $SrMnO_{3-\delta}$ were well solute into host $Bi_{0.5}Na_{0.5}TiO_3$ crystal. Figure 3(a) shows the XRD of pure $Bi_{0.5}Na_{0.5}TiO_3$ samples and $SrMnO_{3-\delta}$-modified $Bi_{0.5}Na_{0.5}TiO_3$ samples with various $SrMnO_{3-\delta}$ concentrations. The peak position and relative intensity of peaks

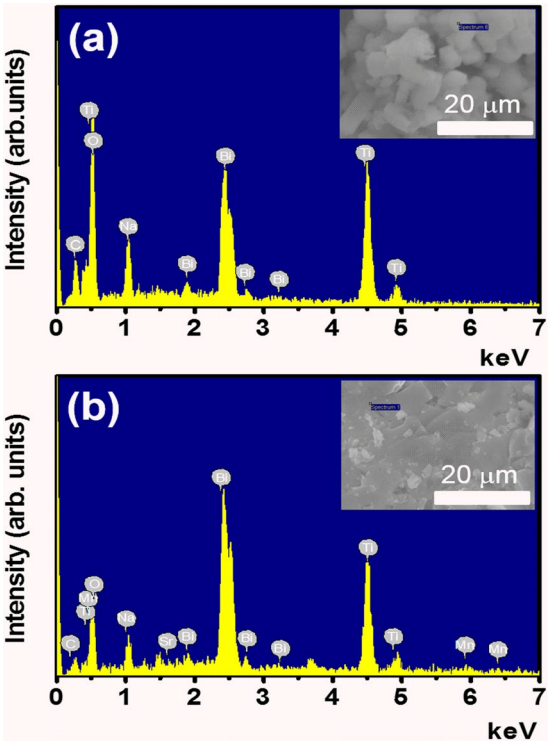

Figure 1. Energy dispersive X-ray spectra of (**a**) pure $Bi_{0.5}Na_{0.5}TiO_3$ samples and (**b**) $SrMnO_{3-\delta}$-modified $Bi_{0.5}Na_{0.5}TiO_3$ samples with 5 mol% $SrMnO_{3-\delta}$ as solid solution. Selection areas for composition element characterization are shown in the inset of each figure.

of pure $Bi_{0.5}Na_{0.5}TiO_3$ samples were indexed as perovskite structure with rhombohedral symmetry. No diffraction peaks of $SrMnO_{3-\delta}$ materials were observed, as shown in the XRD spectra. Besides, the impurity phase was not obtained in the XRD spectra under the resolution of XRD method. The results indicated that the $SrMnO_{3-\delta}$ phase was a good solid solution for host $Bi_{0.5}Na_{0.5}TiO_3$ materials. The influence of solid solution $SrMnO_{3-\delta}$ on the lattice of $Bi_{0.5}Na_{0.5}TiO_3$ materials is shown in Fig. 3(b), wherein the XRD spectra were enlarged in 2θ range from 30°–35° for (012)/(110) peaks. The peak position was overlapped together. Therefore, the peak positions were distinguished using the Lorentzian fitting with r-square of over 0.99. The peak position clearly shifted to a high angle for 3 mol% $SrMnO_{3-\delta}$-modified $Bi_{0.5}Na_{0.5}TiO_3$ materials. Furthermore, addition of $SrMnO_{3-\delta}$ into $Bi_{0.5}Na_{0.5}TiO_3$ materials as solid solution which $SrMnO_{3-\delta}$ over 3 mol.% were resulted in the shrinkage of the lattice parameter as evidence by the shifting of the peak position to a low diffraction angle. The distortion of the lattice parameter was strong evidence for the random substitution of Sr and Mn cations into the host lattice of $Bi_{0.5}Na_{0.5}TiO_3$ materials. The lattice constant of pure $Bi_{0.5}Na_{0.5}TiO_3$ materials and $SrMnO_{3-\delta}$-modified $Bi_{0.5}Na_{0.5}TiO_3$ materials as a function of $SrMnO_{3-\delta}$ concentration is calculated and presented in Fig. 3(c). The results further indicated that the lattice parameter of $Bi_{0.5}Na_{0.5}TiO_3$ compounds was complex in distortion via addition of the different $SrMnO_{3-\delta}$ concentrations. The distorted lattice parameters were possibly understood when the radius of cations in host lattice was identified and compared with substitution impurities. The radius of Sr^{2+} (1.44 Å) cations is larger than that of average *A*-site (Bi^{3+}/Na^{+}) of 1.28 Å (Bi^{3+} (1.17 Å)/Na^{+} (1.39 Å))[34]. However, the complex substitution of Sr^{2+} cations for Bi^{3+} or Na^{+} cations in host lattice resulted in different behaviour, wherein Sr^{2+} cations substituted for Bi^{3+} cations generated the oxygen vacancies, whereas Sr^{2+} cations replacing for Na^{+} cations created the Na-vacancies[35]. Therefore, the Sr substitution in *A*-site was complex in distorted the lattice parameter. In addition, the Mn cations have multivalence states, e.g. as Mn^{2+}, Mn^{3+} and Mn^{4+}. Moreover, the spin state of each valence state influences the radius radii of cation Mn. Mn^{2+} cations have radii of 0.67 Å and 0.830 Å for low-spin and high-spin states, respectively[34]. The Mn^{3+} cations at low-spin and high-spin states have radii of 0.58 Å and 0.645 Å, respectively, whereas the Mn^{4+} cations with only high spin state have radii of 0.530 Å[34]. The Ti^{4+} cations in coordination number of VI have radii of 0.605 Å[34]. Therefore, if Mn cations exist at Mn^{3+} with low-spin state and Mn^{4+}, then substitution for Ti-octahedral structure results in compressor lattice parameter and otherwise expands the lattice parameter of host $Bi_{0.5}Na_{0.5}TiO_3$ materials. Thus, the distortion lattice parameter has a major influence on valence state and spin-state of Mn cations. However, the valence and spin state of Mn cations are very complex and strongly dependent on the chemical environment around the impurities of host materials and on the fabrication condition. Erdem *et al.* reported that Mn^{2+} and Mn^{3+} state existed in $Bi_{0.5}Na_{0.5}TiO_3$-$BaTiO_3$ materials[36]. Meanwhile, Li *et al.* reported that the mix Mn^{2+}/Mn^{4+} valence states are obtained in Mn-doped $Bi_{0.5}Na_{0.5}TiO_3$-$BaTiO_3$-based material[37]. Hejazi *et al.* obtained the multivalence states of Mn such as Mn^{2+}, Mn^{3+} and Mn^{4+} in Mn-doped $Bi_{0.5}Na_{0.5}TiO_3$-based thin films[38]. Anthoniappen *et al.* reported that the Mn^{3+} possibly substituted at Ti-site, whereas Mn^{2+} was locally at the grain boundary[39]. Aksel *et al.* reported that the valence state of Mn changed from Mn^{3+} to Mn^{2+} while increasing the sintering temperature obtained in Mn-doped

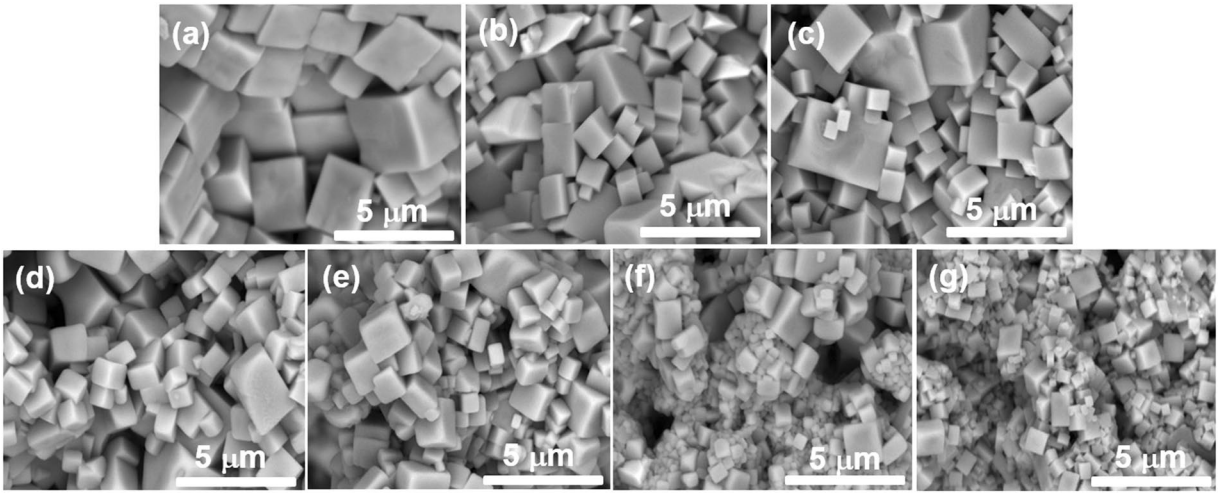

Figure 2. Surface morphology of (**a**) pure $Bi_{0.5}Na_{0.5}TiO_3$, and (**b**–**f**) $SrMnO_{3-\delta}$-modified $Bi_{0.5}Na_{0.5}TiO_3$ with 0.5, 1, 3, 5, 7, and 9 mol.%, respectively.

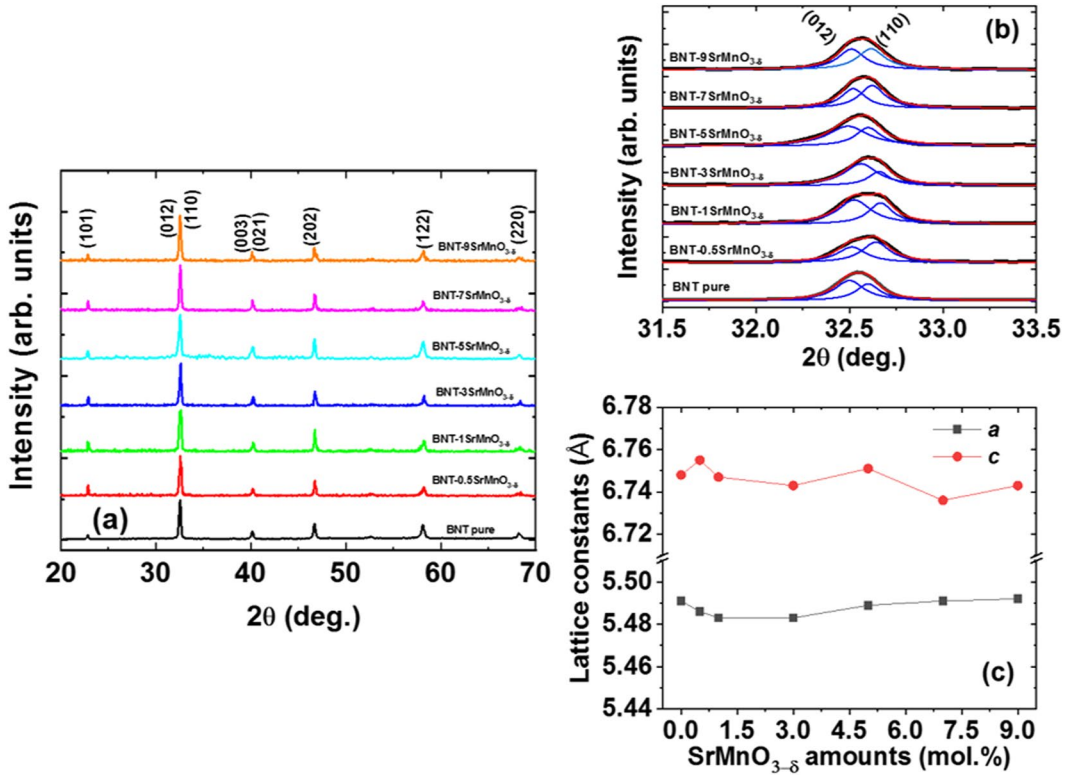

Figure 3. (**a**) X-ray diffraction spectra of pure $Bi_{0.5}Na_{0.5}TiO_3$ and $SrMnO_{3-\delta}$-modified $Bi_{0.5}Na_{0.5}TiO_3$ samples with various concentrations of $SrMnO_{3-\delta}$, (**b**) magnification and deconvolution of X-ray diffraction spectra of pure $Bi_{0.5}Na_{0.5}TiO_3$ and $SrMnO_{3-\delta}$-modified $Bi_{0.5}Na_{0.5}TiO_3$ samples in the 2θ range of 31°–35° with various concentrations, and (**c**) the dependent of lattice parameter of pure $Bi_{0.5}Na_{0.5}TiO_3$ and $SrMnO_{3-\delta}$-modified $Bi_{0.5}Na_{0.5}TiO_3$ samples as function of $SrMnO_{3-\delta}$ as solid solution.

$Bi_{0.5}Na_{0.5}TiO_3$ materials[40]. In addition, due to a lower valence state compared with Ti^{4+}, the incorporation of Mn^{2+} and/or Mn^{3+} into the octahedral site of the structure produces excess negative charges, resulting thereby creating oxygen vacancies maintaining compensate for the maintenance of the overall electrical neutrality. Notably, the radius of oxygen vacancies (1.31 Å), which shrunk the lattice parameter, was smaller than that of oxygen anion (1.4 Å)[41]. The result indicated the XRD peak of host $Bi_{0.5}Na_{0.5}TiO_3$ materials shifted after carrier $SrMnO_{3-\delta}$ was used as the solid solution, thereby providing evidence for the incorporation of Sr and Mn into the host lattice. In other words, the $SrMnO_{3-\delta}$ materials were good solid solutions in $Bi_{0.5}Na_{0.5}TiO_3$ materials.

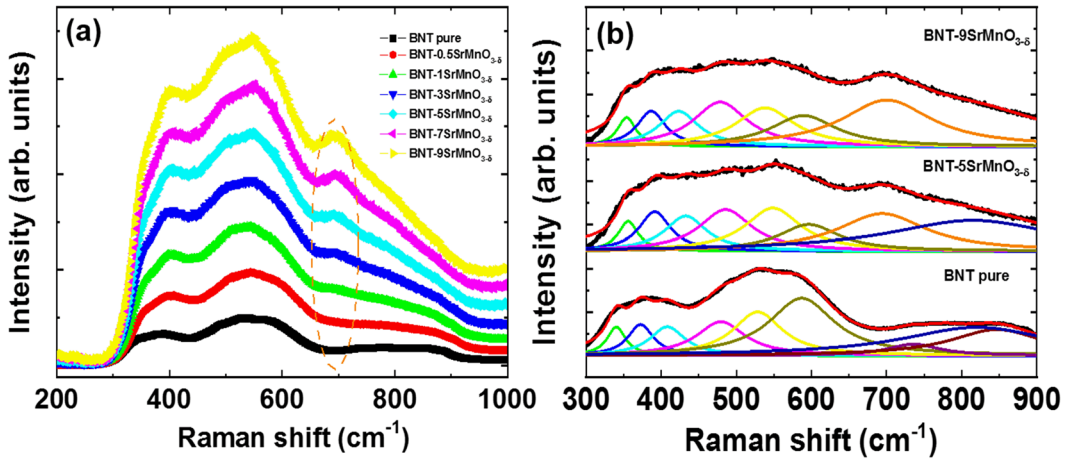

Figure 4. (**a**) Raman scattering spectra of pure $Bi_{0.5}Na_{0.5}TiO_3$ and $SrMnO_{3-\delta}$-modified $Bi_{0.5}Na_{0.5}TiO_3$ samples with various amounts of $SrMnO_{3-\delta}$, and (**b**) deconvolution peak position of pure $Bi_{0.5}Na_{0.5}TiO_3$ and $SrMnO_{3-\delta}$-doped $Bi_{0.5}Na_{0.5}TiO_3$ samples as solid solution with 5 and 9 mol% $SrMnO_{3-\delta}$.

The solute solution of $SrMnO_{3-\delta}$ into host $Bi_{0.5}Na_{0.5}TiO_3$ materials was further confirmed by using Raman scattering studies. Figure 4(a) shows the Raman scattering spectra of pure $Bi_{0.5}Na_{0.5}TiO_3$ and $SrMnO_{3-\delta}$-modified $Bi_{0.5}Na_{0.5}TiO_3$ as solid solution at various $SrMnO_{3-\delta}$ concentrations. The pure $Bi_{0.5}Na_{0.5}TiO_3$ sample exhibited broad band Raman scattering, which resulted from the random distribution of Bi and Na cations at *A*-site in perovskite structure[42]. However, the Raman scattering spectra of $Bi_{0.5}Na_{0.5}TiO_3$ samples can be devised into three main regions in the wavenumber range of 300–1000 cm^{-1}. The addition of $SrMnO_{3-\delta}$addition into $Bi_{0.5}Na_{0.5}TiO_3$ materials caused to the occurrence of new vibration modes. We used the Lorentz fitting to estimate each vibration peak for pure $Bi_{0.5}Na_{0.5}TiO_3$ and $SrMnO_{3-\delta}$-modified $Bi_{0.5}Na_{0.5}TiO_3$ samples. The results of distinguished vibration modes of pure $Bi_{0.5}Na_{0.5}TiO_3$ and $SrMnO_{3-\delta}$-modified $Bi_{0.5}Na_{0.5}TiO_3$ samples with selected $SrMnO_{3-\delta}$ concentration are shown in Fig. 4(b). The nice vibration modes were obtained for pure $Bi_{0.5}Na_{0.5}TiO_3$ samples, and this finding was consistent with the theoretical prediction of Niranjan *et al.*[42]. The addition of the vibration modes at approximately 670 cm^{-1} was obtained for $SrMnO_{3-\delta}$-modified samples, and the intensity of peak increased with the increase of increasing $SrMnO_{3-\delta}$ concentration. The appearance of new vibration modes was suggested for Mn substitution of Ti site to induce the MnO_6 cluster vibration[43,44]. The band observed at approximately 528 cm^{-1} was relative to the breathing modes of TiO_6 octahedral structure, which shifted to a high wavenumber for 5 mol% $SrMnO_{3-\delta}$ dopants then shifted back to low wavenumber for 9 mol% $SrMnO_{3-\delta}$ dopants. This result was consistent with the distorted XRD study for structural distortion of $Bi_{0.5}Na_{0.5}TiO_3$ solid solution with $SrMnO_{3-\delta}$. The Bi/Na–O vibration at low vibration modes was not recorded due to the limitations of our experimental measurement setup. The structural XRD and Raman scattering study of $SrMnO_{3-\delta}$-modified $Bi_{0.5}Na_{0.5}TiO_3$ samples indicated that Mn possible substituted for the Ti site.

Optical properties. The solute solution of $SrMnO_{3-\delta}$ into host $Bi_{0.5}Na_{0.5}TiO_3$ materials results in reduction of optical band gap energy. Figure 5(a) shows the absorbance coefficient as function of absorption photon wavelength for pure $Bi_{0.5}Na_{0.5}TiO_3$ and $SrMnO_{3-\delta}$-modified $Bi_{0.5}Na_{0.5}TiO_3$ samples with various $SrMnO_{3-\delta}$ amounts. The single absorbance edge at approximately 400 nm with a small tail was obtained for pure $Bi_{0.5}Na_{0.5}TiO_3$ samples. The small tail shown in the absorbance spectra of pure $Bi_{0.5}Na_{0.5}TiO_3$ samples was related to self-defect and/or surface defect[45]. The addition of $SrMnO_{3-\delta}$-addition into host $Bi_{0.5}Na_{0.5}TiO_3$ materials changed the optical properties of $Bi_{0.5}Na_{0.5}TiO_3$ materials. The absorbance edge of $SrMnO_{3-\delta}$-modified $Bi_{0.5}Na_{0.5}TiO_3$ samples tended to shift to high wavelength and was not clearly shown due to contribution of absorbance peaks of impurity cations. In addition, the various absorbance peaks were obtained in the absorbance spectra of $SrMnO_{3-\delta}$-modified $Bi_{0.5}Na_{0.5}TiO_3$ samples, which were suggested for various transitions of the transition level energy of impurity cations. $Bi_{0.5}Na_{0.5}TiO_3$ materials with direct transition, wherein in which the electronic band structures were constructed from Bi-6*s*, Ti-4*s* and O-2*p* for conduction band, and the bottom valence band mainly consisting of O-2*p*, Na-3*s* and Ti-3*d* orbitals were theoretically predicted[46,47]. Thus, we used Wood–Tauc method to estimate the value of optical band gap of pure $Bi_{0.5}Na_{0.5}TiO_3$ and $SrMnO_{3-\delta}$-modified $Bi_{0.5}Na_{0.5}TiO_3$ samples. The optical band gap E_g can be obtained from the intercept of $(\alpha h\nu)^{1/n}$ versus photon energy ($h\nu$), where α, ν and h are coefficient absorbance, wavelength and Plank constant, respectively. The band gap values were estimated with $n = 1/2$ for direct transition. The dependence of $(\alpha h\nu)^{1/2}$ to ($h\nu$) for pure $Bi_{0.5}Na_{0.5}TiO_3$ and $SrMnO_{3-\delta}$-modified $Bi_{0.5}Na_{0.5}TiO_3$ samples is shown in Fig. 5(b). E_g of pure $Bi_{0.5}Na_{0.5}TiO_3$ was estimated at approximately 3.07 eV, which were consistent with the recently reported optical band gap of that materials in the range 3.00–3.14 eV[6,48]. $SrMnO_{3-\delta}$ addition into $Bi_{0.5}Na_{0.5}TiO_3$ materials reduced the optical band gap to 1.81 eV for 9 mol% $SrMnO_{3-\delta}$. The details of dependent optical band gap values of $Bi_{0.5}Na_{0.5}TiO_3$ as a function of $SrMnO_{3-\delta}$ amount solid solution into $Bi_{0.5}Na_{0.5}TiO_3$ are shown in the inset of Fig. 5(b). The reduction of optical band gap of $Bi_{0.5}Na_{0.5}TiO_3$ was consistent with the recently reported Mn- or Cr-doped $Bi_{0.5}Na_{0.5}TiO_3$ materials, which resulted from the

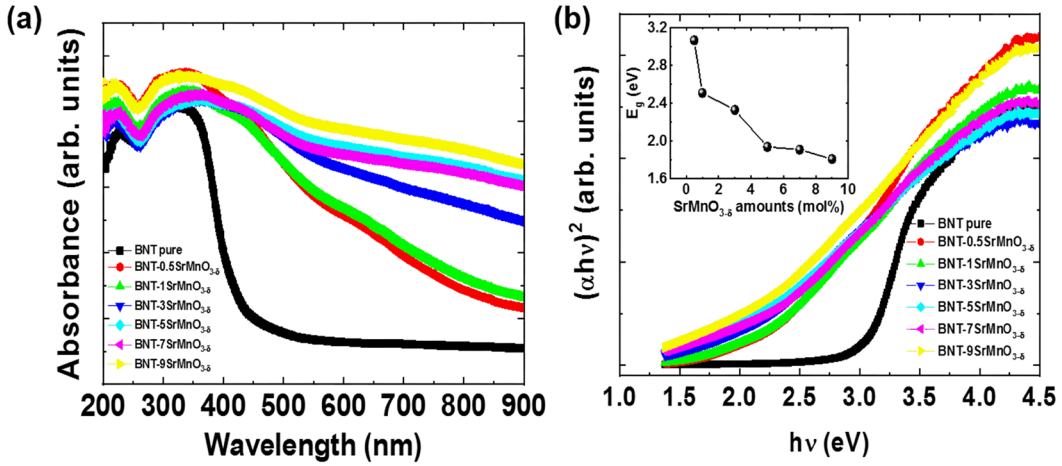

Figure 5. (**a**) Absorbance spectra of pure $Bi_{0.5}Na_{0.5}TiO_3$ and $SrMnO_{3-\delta}$-modified $Bi_{0.5}Na_{0.5}TiO_3$ samples with 0.5, 1, 3, 5, 7, and 9 mol.%, and (**b**) plot of $(\alpha h\gamma)^2$ values as a function of absorbance photon energy ($h\gamma$) for pure $Bi_{0.5}Na_{0.5}TiO_3$ and $SrMnO_{3-\delta}$-modified $Bi_{0.5}Na_{0.5}TiO_3$ samples with various $SrMnO_{3-\delta}$ amounts. Optical band gap energy as a function of $SrMnO_{3-\delta}$-modified $Bi_{0.5}Na_{0.5}TiO_3$ samples as solid solution is shown the inset of (**b**).

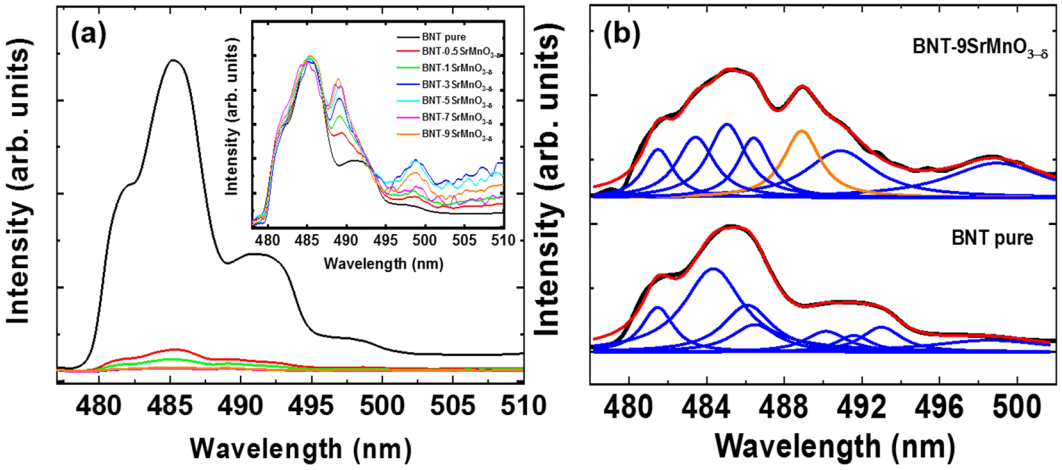

Figure 6. (**a**) Photoluminescence of pure $Bi_{0.5}Na_{0.5}TiO_3$ and $SrMnO_{3-\delta}$-modified $Bi_{0.5}Na_{0.5}TiO_3$ samples with various $SrMnO_{3-\delta}$ concentrations at room temperature, and (**b**) deconvolution photoluminescence peaks for pure $Bi_{0.5}Na_{0.5}TiO_3$ and 9 mol% $SrMnO_{3-\delta}$-modified $Bi_{0.5}Na_{0.5}TiO_3$ samples. Inset of (**a**) shows the comparison of the photoluminescence peak positions of pure $Bi_{0.5}Na_{0.5}TiO_3$ and $SrMnO_{3-\delta}$-modified $Bi_{0.5}Na_{0.5}TiO_3$ samples as solid solution with various concentrations of $SrMnO_{3-\delta}$ after substrate photoluminescence intensity to the unit.

occurrence of local energy state of transition metal in the middle of the electronic band structure of $Bi_{0.5}Na_{0.5}TiO_3$ materials[15,16]. In addition, the created oxygen vacancies caused by unbalance charges between $Mn^{2+/3+}$ with Ti^{4+} and/or Sr^{2+} with Bi^{3+} were flexible enough to reduce the optical band gap, because the oxygen vacancy state was locally near the conduction band[49]. The substitution of Sr^{2+}, possibly acting as a donor, for Na^{+} at *A*-site created the Na-site vacancies.

The addition of $SrMnO_{3-\delta}$ into host $Bi_{0.5}Na_{0.5}TiO_3$ materials as solid solution were suppressed the photoluminescence. Figure 6(a) shows the photoluminescence (PL) emission spectra of pure $Bi_{0.5}Na_{0.5}TiO_3$ and $SrMnO_{3-\delta}$-modified $Bi_{0.5}Na_{0.5}TiO_3$ samples at room temperature. The spectra of pure $Bi_{0.5}Na_{0.5}TiO_3$ samples clearly showed a broad blue emission band within 476–510 nm relative with various transitions. The addition of $SrMnO_{3-\delta}$-addition into $Bi_{0.5}Na_{0.5}TiO_3$ materials as solid solution decreased the intensity of PL emission. In addition, new emission peaks appearing at approximately 489 nm, and the intensity were increased with the increase of increasing $SrMnO_{3-\delta}$ amounts, as shown in the inset of Fig. 6(a) after the standard unit. We tried to distinguish each contribution PL peak via the Lorentz fitting. The results were shown in the examples for undoped $Bi_{0.5}Na_{0.5}TiO_3$ and 9 mol% $SrMnO_{3-\delta}$-modified $Bi_{0.5}Na_{0.5}TiO_3$ samples, as exhibited in Fig. 6(b) for down and up separation figures, respectively. The contribution of various PL peaks is unclear and requires further theoretical investigation. Normally, the PL of ferroelectric materials was not simply from

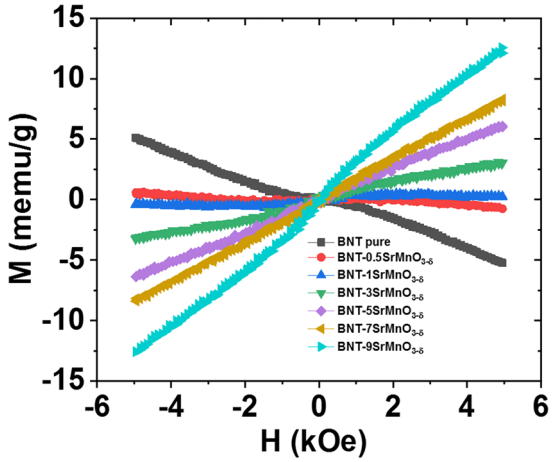

Figure 7. Magnetization as a function of applied magnetic field of pure $Bi_{0.5}Na_{0.5}TiO_3$ samples $SrMnO_{3-\delta}$-modified $Bi_{0.5}Na_{0.5}TiO_3$ samples at room temperature with various $SrMnO_{3-\delta}$ concentrations as solid solution.

band-to-band transition. The combination of photo-electron–hole pairs was difficult to combine due to the separation of the nature polarisation of electrical domain in materials. However, the surface states are often regarded as the dominant cause of luminescence in perovskites. A large number of unsaturated atoms exist on the surface of the perovskites, thereby forming localised levels within the forbidden gaps of the materials. Recently, Bac et al. suggested that the observation of PL of $Bi_{0.5}K_{0.5}TiO_3$ materials was related to the disorder coupled with the tilt of TiO_6-TiO_6 adjacent octahedral structure, thereby resulting in structural distortion and generation of localised electronic levels above the valence band[45]. The re-appearance of new photoluminescent peaks was suggested reliving with the new vibration of MnO_6-TiO_6 or MnO_6-MnO_6 adjacent octahedral structure, as exhibited in the Raman scattering results. The replacement of $Mn^{2+/3+}$ cations for Ti^{4+} cations at *B*-site and Sr^{2+} cation for Bi^{3+} cations at *A*-site created oxygen vacancies, which trapped the electron generated from absorbance photon energy and prevented the recombination of the electron–holes to generate photon, suppressing the PL intensity of $SrMnO_{3-\delta}$-modified $Bi_{0.5}Na_{0.5}TiO_3$ samples. In addition, the substitution of Sr^{2+} cations for the resulting Na^+ cations created the Na vacancies, which also acted as chapping for electrons, thereby reducing the combination of the photon-electron–hole pair.

Magnetic properties. The complex magnetic properties at room temperature of $Bi_{0.5}Na_{0.5}TiO_3$ materials were obtained as function of $SrMnO_{3-\delta}$ solute solution. Figure 7 show the magnetization as function of applied magnetic field (*M–H*) for pure $Bi_{0.5}Na_{0.5}TiO_3$ samples and $SrMnO_{3-\delta}$-modified $Bi_{0.5}Na_{0.5}TiO_3$ sample with various $SrMnO_{3-\delta}$ amounts from 0.5 to 9 mol.%. The pure $Bi_{0.5}Na_{0.5}TiO_3$ materials exhibited the anti-S-shape in *M–H* curves, which resulted from the combination of diamagnetic and weak ferromagnetic properties. The diamagnetic property of $Bi_{0.5}Na_{0.5}TiO_3$ materials behaviour originated from the empty state of Ti^{4+} cations with $3d^0$ states[15,16]. The weak-ferromagnetism observation in pure $Bi_{0.5}Na_{0.5}TiO_3$ materials was possibly related with self-defect and/or surface effects, which were well explained by the first-principle theoretical prediction and experimental achievement[15–17,50]. The anti-*S*-shape in *M–H* curve was obtained for 0.5 mol% $SrMnO_{3-\delta}$ solid solution into $Bi_{0.5}Na_{0.5}TiO_3$ sample. The saturation trend in magnetisation for $SrMnO_{3-\delta}$-doped $Bi_{0.5}Na_{0.5}TiO_3$ with 1 mol% $SrMnO_{3-\delta}$. Further addition of the $SrMnO_{3-\delta}$ concentration into $Bi_{0.5}Na_{0.5}TiO_3$ materials resulted in unsaturation of magnetisation with low applied magnetic field. The slight addition of $SrMnO_{3-\delta}$ into $Bi_{0.5}Na_{0.5}TiO_3$ induced the ferromagnetism due to the interaction of $Mn^{2+/3+}$ through oxygen vacancies ($\square$)[49]. Furthermore, the solid solution of $SrMnO_{3-\delta}$ into $Bi_{0.5}Na_{0.5}TiO_3$ samples enhanced the ferromagnetic ordering due to several favourable $Mn^{2+/3+}$-$\square$-$Mn^{2+/3+}$. In addition, the vacancies of such Na-vacancies, which causes the substitution of Sr^{2+} for Na^+ at *A*-site in perovskite structure, influenced the ferromagnetism in samples[14,17]. Moreover, if Sr^{2+} cations substituted for Bi^{3+} cations were possible resulted in changing the valence state of Ti^{4+} to Ti^{3+} state cause of enhancement the number of oxygen vacancies[35]. Our recently predicted that the Ti^{3+}-defects state in $Bi_{0.5}K_{0.5}TiO_3$ materials was strong induced the ferromagnetism[51]. However, the unsaturation in magnetisation as a function of low applied magnetic field via further addition of $SrMnO_{3-\delta}$ (over 3 mol%) into $Bi_{0.5}Na_{0.5}TiO_3$ materials was possibly related to the isolation of Mn cations, which favoured of paramagnetic property or/and interaction of polaron ($Mn^{2+/3+}$-$\square$-$Mn^{2+/3+}$) vs. ($Mn^{2+/3+}$-$\square$-$Mn^{2+/3+}$), which favoured the antiferromagnetic-like materials[52]. The magnetisation of 9 mol%-doped $Bi_{0.5}Na_{0.5}TiO_3$ samples was achieved at approximately 12.5 memu/g at room temperature, which was greatly enhanced compared with pure $Bi_{0.5}Na_{0.5}TiO_3$ materials[15,16]. The values were also larger than that of Mn-, Fe-, Cr- and Co-doped $Bi_{0.5}Na_{0.5}TiO_3$ materials[15,16,18,19]. Thus, we suggested that the co-modification at *A*-site and *B*-site via alkalize and transition metals, respectively, displayed higher performance magnetic properties than single transition metal-doped $Bi_{0.5}Na_{0.5}TiO_3$ materials. However, the role of *A*-site-modification on the magnetic properties of $Bi_{0.5}Na_{0.5}TiO_3$-dope-material with transition metal needs further theoretical calculated investigation.

Discussion

The new system $Bi_{0.5}Na_{0.5}TiO_3$-$SrMnO_{3-\delta}$ solid solution materials were fabricated via sol–gel method. X-ray diffraction and Raman scattering were used to study the structure of pure $Bi_{0.5}Na_{0.5}TiO_3$ and $SrMnO_{3-\delta}$-modified $Bi_{0.5}Na_{0.5}TiO_3$ materials with various $SrMnO_{3-\delta}$ amount, providing that all samples followed the crystal structural symmetry of host rhombohedral structure of $Bi_{0.5}Na_{0.5}TiO_3$ materials. This phenomenon indicated that the $SrMnO_{3-\delta}$ materials were good solid solution in host $Bi_{0.5}Na_{0.5}TiO_3$ crystal structure. The Sr and Mn cations were diffused to random incorporation with host lattice of $Bi_{0.5}Na_{0.5}TiO_3$ crystal to form as solid solution, resulting in complex-distorted structure. The random distribution of Sr^{2+} cations into *A*-site of $Bi_{0.5}Na_{0.5}TiO_3$ materials was possibly different, indicating that Sr^{2+} cations substituted for Bi^{3+} cations generate the oxygen vacancies, whereas the Sr^{2+} cations replaced for Na^{+} create the Na vacancies. The presentation of complex defects in $Bi_{0.5}Na_{0.5}TiO_3$ materials during solid solution of $SrMnO_{3-\delta}$ reduced the optical band gap values from approximately 3.07 eV to 1.18 eV for 9 mol% $SrMnO_{3-\delta}$ solid solution. The absorbance spectroscopy of $SrMnO_3$-modified $Bi_{0.5}Na_{0.5}TiO_3$ materials exhibited the multi-absorbance peaks in visible absorbance range, presenting the multivalence state of Mn cations, such as Mn^{2+}, Mn^{3+}, and Mn^{4+}. Thus, the modified *B*-site by multivalence state of Mn cations also possibly exhibited the different interactions, wherein the $Mn^{2+/3+}$ cation interaction through the oxygen vacancies ($Mn^{2+/3+}$-□-$Mn^{2+/3+}$) resulted in ferromagnetic ordering, whereas Mn^{4+} cation interaction through oxygen (Mn^{4+}-O^{2-}-Mn^{4+}) was favourable to antiferromagnetic ordering. Mn cation isolates incorporated with host lattice displayed the paramagnetic behaviour. The possible antiferromagnetic-like structure started to occur when the Mn cations were rich enough to bind together the superinteraction of pair ($Mn^{2+/3+}$-□-$Mn^{2+/3+}$) vs. ($Mn^{2+/3+}$-□-$Mn^{2+/3+}$). Therefore, by controlling the $SrMnO_{3-\delta}$ concentration doping in host lattice $Bi_{0.5}Na_{0.5}TiO_3$ materials, the magnetic properties of $Bi_{0.5}Na_{0.5}TiO_3$ materials were tuned from compensationof diamagnetic and weak ferromagnetic property of pure materials to typical ferromagnetism behaviour and at the end of combination of paramagnetism/antiferromagnetism-like versus ferromagnetism with the increase of the $SrMnO_{3-\delta}$ amount solid solution into host $Bi_{0.5}Na_{0.5}TiO_3$ materials. We expected that co-modification at the *A*-site and *B*-site in lead-free ferroelectric perovskite ABO_3 materials via alkali earth and transition metals, respectively, resulted in great enhancement of the ferromagnetism than that of contribution of self-defect and/or surface effects, or by using single transition metal dopants. We also expected that our method opened the new way to develop injection ferromagnetism in lead-free ferroelectric materials, such as $BaTiO_3$-based and (K,Na)NbO_3-based family, by using solid solution method. The observation of tuneable magnetic and optical properties of lead-free ferroelectric material was promising for application to green electronic devices.

Methods

Sample preparation. The pure $Bi_{0.5}Na_{0.5}TiO_3$ compounds were fabricated from material source of bismuth nitrate pentahydrate ($Bi(NO_3)_3.5H_2O$), sodium nitrate ($NaNO_3$) and tetraisopropoxytitanium (IV, $C_{12}H_{28}O_4Ti$). The $Bi(NO_3)_3{\cdot}5H_2O$ and $NaNO_3$ were weighed and distinguished in acetic acid and de-ions water H_2O (V_{H2O}:$V_{CH3COOH} = 5$: 1). The acetylacetone was added dropwise before the addition of $C_{12}H_{28}O_4Ti$. The solution was magnetically stirred at approximately 3 h and heated followed by at100 °C to prepare the gel. The $(x)SrMnO_{3-\delta} + (1-x)Bi_{0.5}Na_{0.5}TiO_3$ ($x = 0.5$, 1, 3, 5, 7, 9 mol%) compounds were fabricated by using a similar method of fabrication with pure $Bi_{0.5}Na_{0.5}TiO_3$. However, the starting materials were $Sr(NO_3)_2$ and a solution of $Mn(NO_3)_3$ (60%). These materials were weighed, and the solution was added by estimating the dopant concentrations. The gels were ground and annealed for 5 h at 800 °C and then naturally cooled to room temperature. Extra sodium was added at approximately 50 mol% to prevent sodium loss during gelling and annealing processing[24,25].

Sample characterization. The surface morphology and presentation of the elements in samples was measured by Energy Dispersive X-ray analysis (EDX, S-4800 Hitachi). The chemical composition of pure $Bi_{0.5}Na_{0.5}TiO_3$ samples and $SrMnO_{3-\delta}$-modified $Bi_{0.5}Na_{0.5}TiO_3$ compounds was further confirmed by using an electron probe micro-analyzer (EPMA, Shimadzu EPMA 1600). The sample powder was ground for characterisation via X-ray diffraction (XRD, Brucker D8 Advance) and Raman scattering (with a 475 nm LASOS laser and a DU420A-Oe defector) to analyse the crystal structure and vibration mode of the atom, respectively. The absorbance spectroscopy and photoluminescent properties of pure and $SrMnO_{3-\delta}$-modified $Bi_{0.5}Na_{0.5}TiO_3$ compounds were measured by using Ultraviolet–Visible spectroscopy (UV–Vis, Jasco V-670) and photoluminescence (exciter with 475 m LASOS laser and a DU420A-Oe defector), respectively. The magnetic properties were studied using a Vibrating Sample Magnetometry (VSM, Lakeshore 7404) at room temperature, respectively. Finally, we used X-ray photoelectron spectroscopy (XPS, Thermofisher, a twin anode X-ray source (Al Kα, hν =1686.6 eV) gun and monochromatic gun) to determine the valence state of the cations in the pure $Bi_{0.5}Na_{0.5}TiO_3$ and 9 mol.% $SrMnO_{3-\delta}$-modified $Bi_{0.5}Na_{0.5}TiO_3$ samples, as shown in Figure S1 and Figure S2, respectively, in suplimental data. The X-ray diffraction peaks, Raman scattering peaks, XPS peaks and photoluminescence peaks were distinguished by using Lorentzian fitting with r-square over 0.99.

Received: 18 February 2019; Accepted: 7 November 2019;
Published online: 03 December 2019

References

1. Reichmann, K., Feteira, A. & Li, M. Bismuth sodium titanate based materials for piezoelectric actuato. *Materials* **8**, 8467–8495 (2015).
2. Quan, N. D., Bac, L. H., Thiet, D. V., Hung, V. N. & Dung, D. D. Current development in lead-free-based piezoelectric materials. *Adv. Mater. Sci. Eng.* **2014**, 365391 (2014).
3. Smolenskii, G. A., Isupov, V. A., Agranovskaya, A. I. & Krainik, N. N. New ferroelectrics of. complex composition. *Sov. Phys. Solid State* **2**, 2651–2654 (1961).

4. Guo, F. F. *et al*. Morphotropic phase boundary and electric properties in $(1-x)Bi_{0.5}Na_{0.5}TiO_3$-$xBiCoO_3$ lead-free piezoelectric ceramics. *J. Appl. Phys.* **111**, 124113 (2012).
5. Pattipaka, S., Mahesh, P. & Pamu, D. Structural and dielectric properties of lead free $Bi_{0.5}Na_{0.5}TiO_3$ ceramics. *AIP Conf. Proc.* **1728**, 020352 (2016).
6. Thanh, L. T. H. *et al*. Influence of sintering temperature on phase formation and optical properties of lead-free ferroelectric $Bi_{0.5}Na_{0.5}TiO_3$. *materials. J. Sci. Tech.* **54**, 104–111 (2016).
7. Hong, C. H. *et al*. Lead-free piezoceramics – Where to move on? *J. Materomics* **2**, 1–24 (2016).
8. Koruza, J. *et al*. Requirements for the transfer of lead-free piezoceramics into application. *J. Materomics* **4**, 13–26 (2018).
9. Liu, F., Wahyudi, O. & Li, Y. A new $Bi_{0.5}Na_{0.5}TiO_3$ based lead-free piezoelectric system with calculated end-member $Bi(Zn_{0.5}Hf_{0.5})O_3$. *J. Appl. Phys.* **115**, 114101 (2014).
10. Ullah, A. *et al*. High strain response in ternary $Bi_{0.5}Na_{0.5}TiO_3$–$BaTiO_3$–$Bi(Mn_{0.5}Ti_{0.5})O_3$ solid solutions. *RSC Adv.* **6**, 63915–63921 (2016).
11. Bai, W. *et al*. Structure and electromechanical properties in $Bi_{0.5}Na_{0.5}TiO_3$-based lead-free piezoceramics with calculated end-member $Bi(Ni_{0.5}Ti_{0.5})O_3$. *J. European Ceram. Soc.* **35**, 3457–3466 (2015).
12. Bai, W. *et al*. Phase evolution and correlation between tolerance factor and electromechanical properties in BNT-based ternary perovskite compounds with calculated end-member $Bi(Me_{0.5}Ti_{0.5})O_3$ (Me = Zn, Mg, Ni, Co). *Dalton Trans.* **45**, 14141–14153 (2016).
13. Li, H. L. *et al*. Grain size dependent electrostrain in $Bi_{1/2}Na_{1/2}TiO_3$-$SrTiO_3$ incipient piezoceramics. *J. European Ceram. Soc.* **36**, 2849–2853 (2016).
14. Ju, L. *et al*. Room-temperature magnetoelectric coupling in nanocrystalline $Na_{0.5}Bi_{0.5}TiO_3$. *J. Appl. Phys.* **116**, 083909 (2014).
15. Thanh, L. T. H. *et al*. Origin of room temperature ferromagnetism in Cr-doped lead-free ferroelectric $Bi_{0.5}Na_{0.5}TiO_3$ materials. *J. Electron. Mater.* **46**, 3367–3372 (2017).
16. Thanh, L. T. H. *et al*. Making room-temperature ferromagnetism in lead-free ferroelectric $Bi_{0.5}Na_{0.5}TiO_3$ materials. *Mater. Lett.* **186**, 239–242 (2017).
17. Zhang, Y., Hu, J., Gao, F., Liu, H. & Qin, H. Ab initio calculation for vacancy-induced magnetism in ferroelectric $Na_{0.5}Bi_{0.5}TiO_3$. *Comput. Theor. Chem.* **967**, 284–288 (2011).
18. Wang, Y. *et al*. Room-temperature ferromagnetism in Fe-doped $Na_{0.5}Bi_{0.5}TiO_3$. *crystals. Mater. Sci. Poland* **27**, 471–476 (2009).
19. Wang, Y. *et al*. Room-temperature ferromagnetism in Co-doped $Na_{0.5}Bi_{0.5}TiO_3$: diluted magnetic ferroelectrics. *J. Alloys Compound.* **475**, L25–L30 (2009).
20. Wu, X. *et al*. Luminescent–electrical–magnetic performances of sol–gel-derived Ni^{2+}-modified $Bi_{0.5}Na_{0.5}TiO_3$. *J. Mater. Sci.: Mater. Electron.* **28**, 12021–12025 (2017).
21. Kumari, M., Singh, A., Gupta, A., Rrahash, C. & Chatterjee, R. Self-biased large magnetoelectric coupling in co-sintered $Bi_{0.5}Na_{0.5}TiO_3$ based piezoelectric and $CoFe_2O_4$ based magnetostrictive bilayered composite. *J. Appl. Phys.* **116**, 244101 (2014).
22. Manjusha, Y. K. L., Adhlakha, N., Shah, J. & Kotnala, R. K. Strain mediated magnetoelectric coupling induced in $(x)Bi0.5Na_{0.5}TiO_3$-$(1-x)MgFe_2O_4$ composites. *Physica B* **514**, 41–50 (2017).
23. Zhang, R. F., Deng, C. Y., Ren, L., Li, Z. & Zhou, J. P. Ferroelectric, ferromagnetic, and magnetoelectric properties of multiferroic $Ni_{0.5}Zn_{0.5}Fe_2O_4$–$BaTiO_3$ composite ceramics. *J. Electron. Mater.* **43**, 1043–1047 (2014).
24. Hung, N. T. *et al*. Room-temperature ferromagnetism in Fe-based perovskite solid solution in lead-free ferroelectric $Bi_{0.5}Na_{0.5}TiO_3$ materials. *J. Magn. Magn. Mater.* **451**, 183–186 (2018).
25. Hung, N. T. *et al*. Structural, optical, and magnetic properties of $SrFeO_{3-\delta}$-modified $Bi_{0.5}Na_{0.5}TiO_3$ materials. *Physica B* **531**, 75–78 (2018).
26. Kuroda, K., Shinozaki, K., Uematsu, K., Mizutani, N. & Kato, M. Oxygen-deficiency-induced polymorphohs and electrical conductivity of $SrMnO_{3-x}$. *J. American Ceram. Soc.* **63**, 109–110 (1980).
27. Kobayashi, S. *et al*. Quantitative analyses of oxidation states for cubic $SrMnO_3$ and orthorhombic $SrMnO_{2.5}$ with electron energy loss spectroscopy. *J. Appl. Phys.* **108**, 124903 (2010).
28. Belik, A. A. *et al*. Crystal structure and magnetic properties of 6H-$SrMnO_3$. *Phys. Rev. B* **84**, 094438 (2011).
29. Suescun, L., Chmaissem, O., Mais, J., Daborwski, B. & Jorgensen, J. D. Crystal structures, charge and oxygen-vacancy ordering in oxygen deficient perovskites $SrMnO_x$ ($x < 2.7$). *J. Solid State Chem.* **180**, 1698–1707 (2007).
30. Kamba, S. *et al*. Strong spin-phonon coupling in infrared and Raman spectra of $SrMnO_3$. *Phys. Rev. B* **89**, 064308 (2014).
31. Rahman, M., Zhou, K. C., Nie, Y. Z. & Guo, G. H. Electronic structure and magnetism of layered compounds $SrBO_2$ (B = Ni, Co, Mn): A theoretical investigation. *Solid State Commun.* **266**, 6–10 (2017).
32. Zhou, C., Liu, X., Li, W. & Yuan, C. Structure and piezoelectric properties of $Bi_{0.5}Na_{0.5}TiO_3$-$Bi_{0.5}K_{0.5}TiO_3$-$BiFeO_3$ lead-free piezoelectric ceramics. *Mater. Chem. Phys.* **114**, 832 (2009).
33. Tuan, N. H. *et al*. Structural, optical, and magnetic properties of lead-free ferroelectric $Bi_{0.5}K_{0.5}TiO_3$ solid solution with $BiFeO_3$ materials. *J. Electron. Mater.* **46**, 3472–3478 (2017).
34. Shannon, R. D. & Prewitt, C. T. Effective ionic radii in oxides and fluorides. *Acta Cryst. B* **25**, 925–946 (1969).
35. Qiao, Y. *et al*. Local order and oxygen ion conduction induced high-temperature colossal permittivity in lead-free $Bi_{0.5}Na_{0.5}TiO_3$-based systems. *ACS Appl. Energy Mater.* **1**, 956–962 (2018).
36. Erdem, E. *et al*. analysis of MnO_2-doped $[Bi_{0.5}Na_{0.5}]TiO_3$-$BaTiO_3$ piezoelectric ceramics – manganese oxidation states and materials 'hardening'. *Ferroelectrics* **428**, 116–121 (2012).
37. Li, F., Zhai, J., Shen, B., Liu, X. & Zeng, H. Simultaneously high-energy storage density and responsivity in quasi-hysteresis-free Mn-doped $Bi_{0.5}Na_{0.5}TiO_3$-$BaTiO_3$-$(Sr_{0.7}Bi_{0.2}\square_{0.1})TiO_3$ ergodic relaxor ceramics. *Mater. Res. Lett.* **6**, 345–352 (2018).
38. Hejazi, M. H., Taghaddos, E. & Safari, A. Reduced leakage current and enhanced ferroelectric properties in Mn-doped $Bi_{0.5}Na_{0.5}TiO_3$-based thin films. *J. Mater. Sci.* **48**, 3511–3516 (2013).
39. Anthoniappen, J. *et al*. Raman spectra and structural stability in B-site manganese doped $(Bi_{0.5}Na_{0.5})_{0.925}Ba_{0.075}TiO_3$ relaxor ferroelectric ceramics. *J. European Ceram. Soc.* **35**, 3495–3506 (2015).
40. Aksel, E. *et al*. Processing of manganese-doped $[Bi_{0.5}Na_{0.5}]TiO_3$ ferroelectrics: reduction and oxidation reactions during calcination and sintering. *J. Am. Ceram. Soc.* **94**, 1363–1369 (2011).
41. Chatzichristodoulou, C., Norby, P., Hendriksen, P. V. & Mogensen, M. B. Size of oxide vacancies in fluorite and perovskite structured oxides. *J. Electroceram.* **34**, 100–107 (2015).
42. Niranjan, M. K., Karthik, T., Asthana, S., Pan, J. & Waghmare, U. V. Theoretical and experimental investigation of raman modes, ferroelectric and dielectric properties of relaxor $Na_{1/2}Bi_{1/2}TiO_3$. *J. Appl. Phys.* **113**, 194106 (2013).
43. Guowei, Z., Youngsoo, K., Tianduo, L. & Guiying, X. Sol-gel preparation and spectroscopic study of the pyrophanite $MnTiO_3$ nanoparticles. *Sci. China Ser. B. Chem.* **48**, 210–215 (2005).
44. Awan, M. Q. *et al*. limit and its effects on physical properties of lead-free $Bi_{0.5}Na_{0.5}TiO_3$ ceramics. *Ceram. Inter.* **44**, 12767–12773 (2018).
45. Bac, L. H. *et al*. Tailoring the structural, optical properties and photocatalytic behavior of ferroelectric $Bi_{0.5}K_{0.5}TiO_3$ nanopowders. *Mater. Lett.* **164**, 631–635 (2016).
46. Baedi, J. & Mircholi, F. The study of the electronical properties of $BiTiO_3$ crystal by substitution of Na atom. *Optik* **127**, 1503–1506 (2016).
47. Baedi, J., Gholampur, S. & Mircholi, F. The study of the electronic properties of $Bi_{0.5}Na_{0.5}TiO_3$, $Bi_{0.5}Na_{0.5}Ti_{0.5}Zr_{0.5}O_3$ and $Bi_{0.5}Na_{0.5}ZrO_3$ compounds and comparing their structures. *Optical Mater.* **67**, 44–51 (2017).

48. Thanh, L. T. H., Tuan, N. H., Bac, L. H. & Dung, D. D. Influence of fabrication condition on the microstructural and optical properties of lead-free ferroelectric $Bi_{0.5}Na_{0.5}TiO_3$ materials. *Commun. Phys.* **26**, 51–57 (2016).
49. Tuan, N. H. *et al*. Defect induced room temperature ferromagnetism in lead-free ferroelectric $Bi_{0.5}K_{0.5}TiO_3$ materials. *Physica B* **532**, 108–114 (2018).
50. Ju, L. *et al*. Room-temperature magnetoelectric coupling in nanocrystalline $Na_{0.5}Bi_{0.5}TiO_3$. *J. Appl. Phys.* **116**, 083909 (2014).
51. Tuan, N. H. *et al*. Theoretical and experimental studies on the influence of Cr incorporation on the structural, optical, and magnetic properties of $Bi_{0.5}K_{0.5}TiO_3$ materials. *J. Sol-Gel Sci. Tech.* **87**, 528–536 (2018).
52. Tuan, N. H., Linh, N. H., Odkhuu, D., Trung, N. N. & Dung, D. D. Microstructural, optical, and magnetic properties of $BiCoO_3$-modified $Bi_{0.5}K_{0.5}TiO_3$. *J. Electron. Mater.* **47**, 3414–3420 (2018).

Acknowledgements

This work was financially supported by The Ministry of Science and Technology, Viet Nam, under project number ĐTĐLCN.29/18.

Author contributions

D.D.D. and D.O. conceived the idea and designed the experiments. N.T.H. performed the experiments and measurements. D.D.D. wrote the paper. D.O. reviewed and commented on the paper. All authors discussed the results and commented on the manuscript.

Competing interests

The authors declare no competing interests.

Additional information

Supplementary information is available for this paper at https://doi.org/10.1038/s41598-019-54172-4.

Correspondence and requests for materials should be addressed to D.D.D. or D.O.

Reprints and permissions information is available at www.nature.com/reprints.

Publisher's note Springer Nature remains neutral with regard to jurisdictional claims in published maps and institutional affiliations.